

**Supporting Information for
An Experimental and Theoretical Comparison of the O K-Edge Non-
Resonant Inelastic X-ray Scattering and X-ray Absorption Spectrum of
NaReO₄**

Joseph A. Bradley,^{1,2} Ping Yang⁴, Enrique R. Batista,^{*1} Kevin S. Boland,¹ Carol J. Burns,¹ David L. Clark,¹ Steven D. Conradson,¹ Stosh A. Kozimor,^{*1} Richard L. Martin,^{*1} Gerald T. Seidler,^{*2} Brian L. Scott,¹ David K. Shuh,^{*3} Tolek Tyliszczak,³ Marianne P. Wilkerson,¹ Laura E. Wolfsberg¹

¹ Los Alamos National Laboratory, Los Alamos, New Mexico 87545 (U.S.A.)

² Department of Physics, University of Washington, Seattle WA, 98195

³ Chemical Sciences Division and Advanced Light Source, Lawrence Berkeley National Laboratory, Berkeley CA, 94720

⁴ W.R. Wiley Environmental Molecular Sciences Laboratory, Pacific Northwest National Laboratory, Richland, WA 99352

E-mail: stosh@lanl.gov

- **Figure S1.** A plot of energy vs. normalized intensity for the O K-edge non-resonant inelastic X-ray scattering (NRIXS) spectrum of NaReO₄ that had been encapsulated in polystyrene. S2
- **Figure S2.** A plot of energy vs. normalized intensity for the O K-edge X-ray absorption spectrum of NaReO₄ that had been encapsulated in polystyrene obtained using fluorescence yield detection. S3
- **Figure S3.** A plot of energy vs. normalized intensity for the O K-edge X-ray absorption spectrum of a single particle of NaReO₄, which is shown in the insert, using scanning transmission X-ray microscopy. S4
- **Figure S4.** The TD-DFT calculated spectrum (red) that shows contributions from O 1s electronic excitations to molecular orbitals that primarily consist of Re s (green), p (blue), and d (pink) orbitals. S5
- **Figure S5.** Analysis of the sensitivity of the predicted spectrum to some simulation parameters such as functional, basis set, and methodology S6
- **Figure S6.** Density of unoccupied states in a crystal simulation of NaReO₄ calculated with hybrid DFT and decomposed in angular momentum components S7
- **Figure S7.** Molecular orbitals for ReO₄⁻ calculated at the B3LYP optimized structure, Re-O=1.751 Å. (expt. Re-O=1.722 Å). S8
- **Table S1.** The calculated bond lengths and charge for the optimized structure of the ReO₄¹⁻ anion. S9
- **Table S2.** Orbital composition for representative occupied and unoccupied orbitals for ReO₄⁻ orbital contributions (B3LYP//Stuttgart, optimized structure, Gaussian 03). S10
- **References** S11

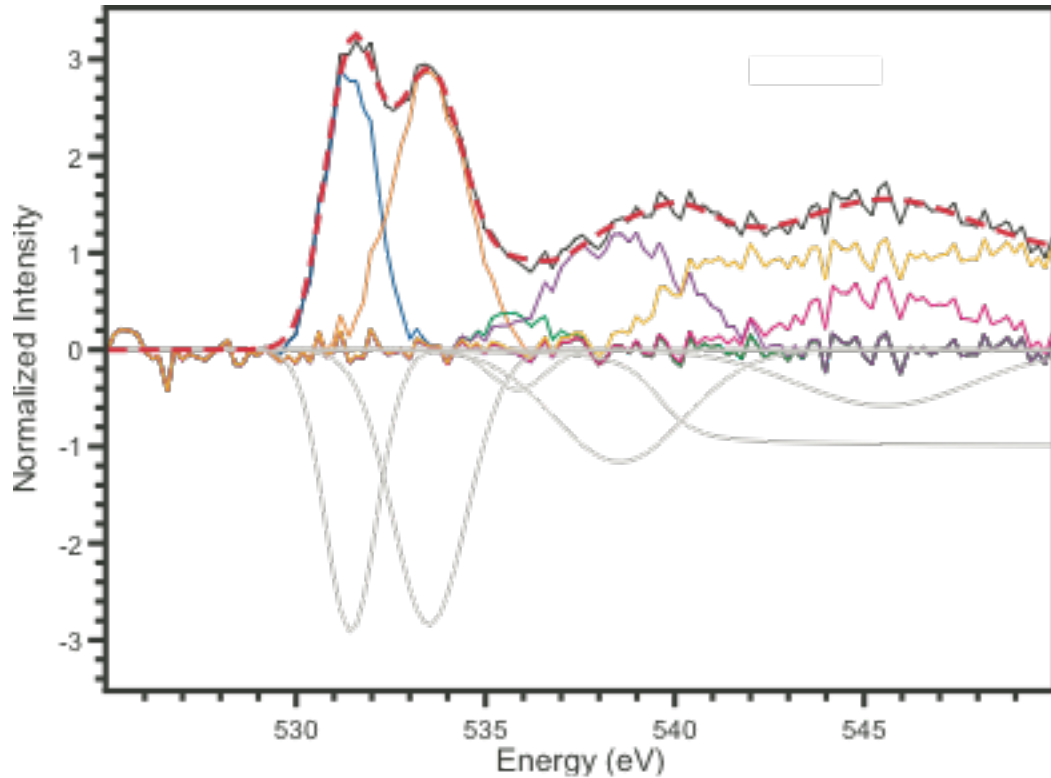


Figure S1. A plot of energy vs. normalized intensity for the O K-edge non-resonant inelastic X-ray scattering (NRIXS) spectrum of NaReO_4 that had been encapsulated in polystyrene. The experimental data (black) and curve fit (red dashes) are compared with the residual features^a (blue, orange, green, purple, pink, and yellow) and the negative amplitudes of the Gaussian functions (gray) used to generate the fit.

^a Residual features are obtained by subtracting the functions used to generate the fit, with the exception of the function used to model the feature of interest, from the data.

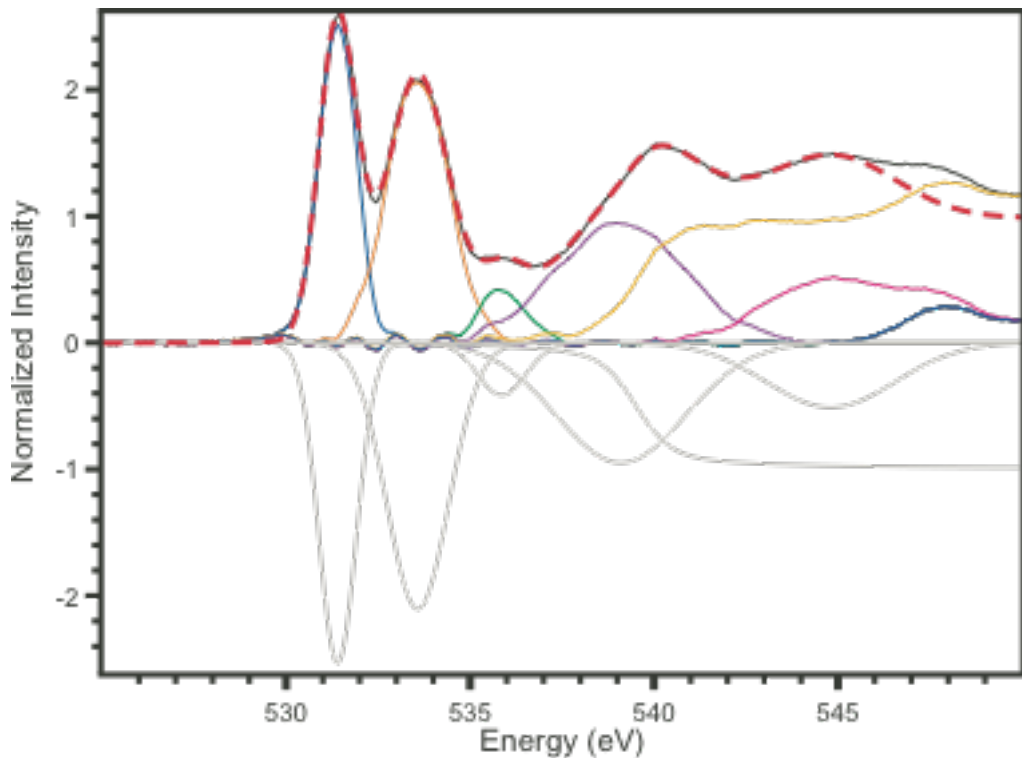


Figure S2. A plot of energy vs. normalized intensity for the O K-edge X-ray absorption spectrum of NaReO_4 that had been encapsulated in polystyrene obtained using fluorescence yield detection. The experimental data (black) and curve fit (red dashes) are compared with the residual features^a (blue, orange, green, purple, pink, and yellow) and the negative amplitudes of the Gaussian functions (gray) used to generate the fit.

^a Residual features are obtained by subtracting the functions used to generate the fit, with the exception of the function used to model the feature of interest, from the data.

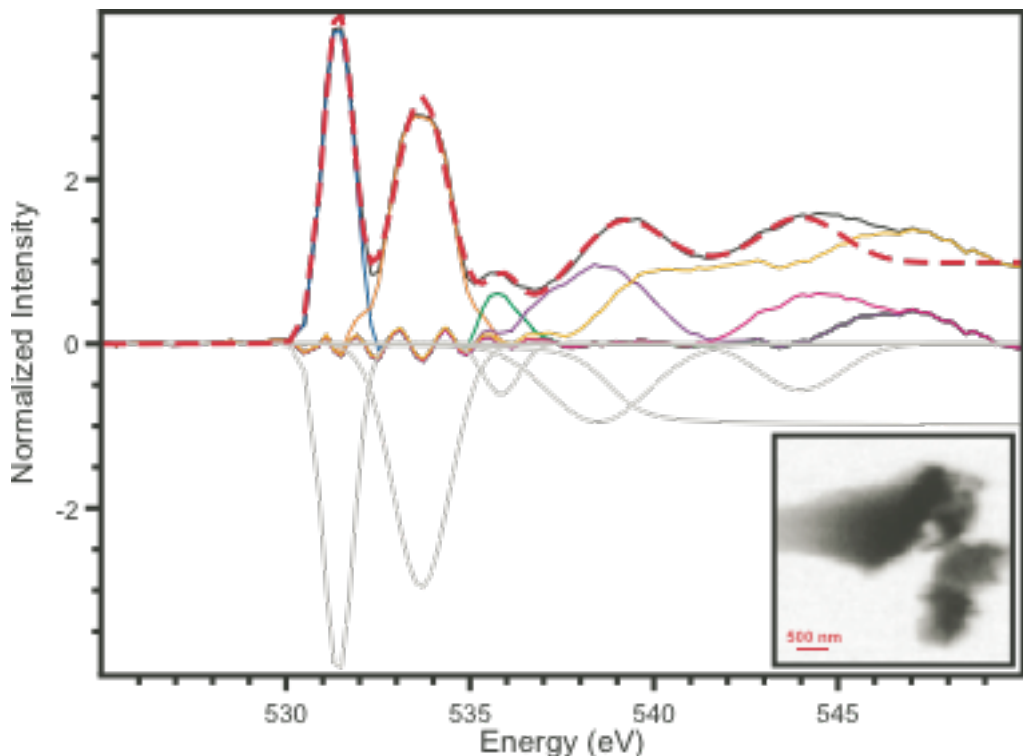


Figure S3. A plot of energy vs. normalized intensity for the O K-edge X-ray absorption spectrum of a single particle of NaReO₄, which is shown in the insert, using scanning transmission X-ray microscopy. The experimental data (black) and curve fit (red dashes) are compared with the residual features^a (blue, orange, green, purple, pink, and yellow) and the negative amplitudes of the Gaussian functions (gray) used to generate the fit.

^a Residual features are obtained by subtracting the functions used to generate the fit, with the exception of the function used to model the feature of interest, from the data.

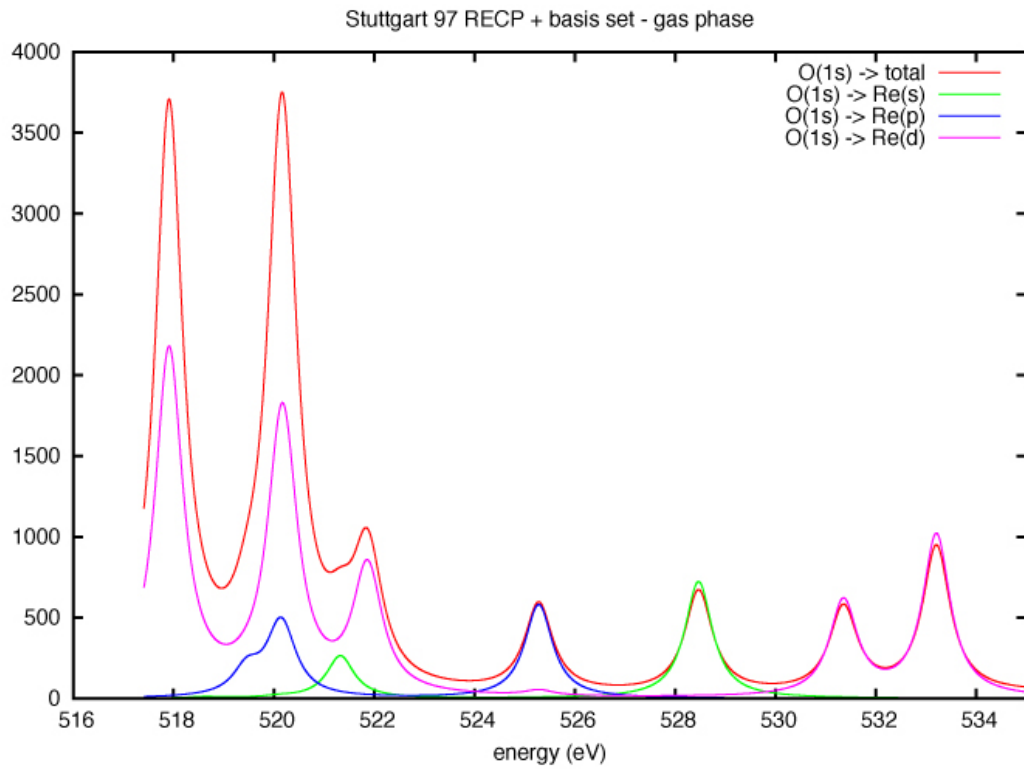


Figure S4. The TD-DFT calculated spectrum (red) that shows contributions from O 1s electronic excitations to molecular orbitals that primarily consist of Re s (green), p (blue), and d (pink) orbitals.

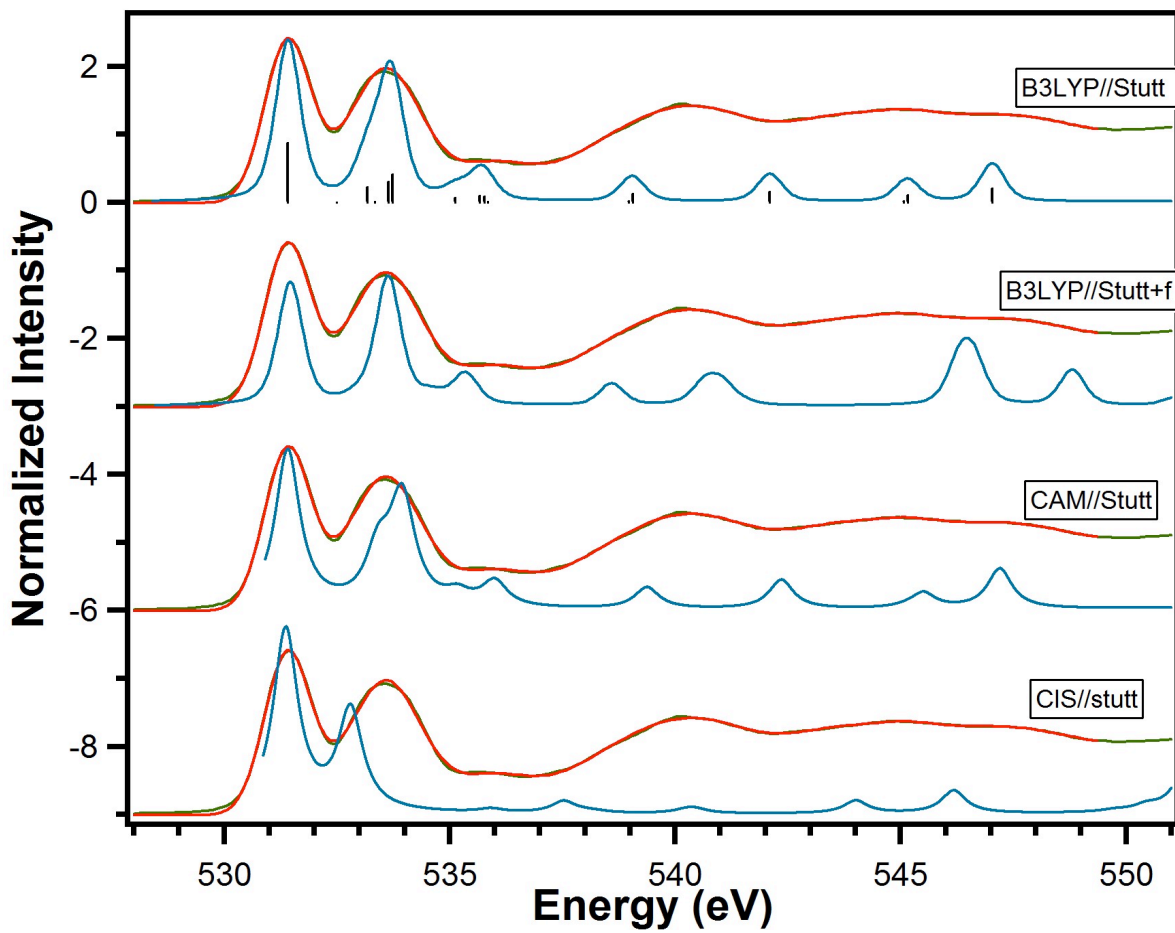


Figure S5. Comparison of predicted spectrum with experimental one to test the reliability of the computational interpretation. Spectra calculated with the following levels of theory are overlaid: B3LYP, adding a full f shell, using CAM-B3LYP, and configuration interaction with single excitations.

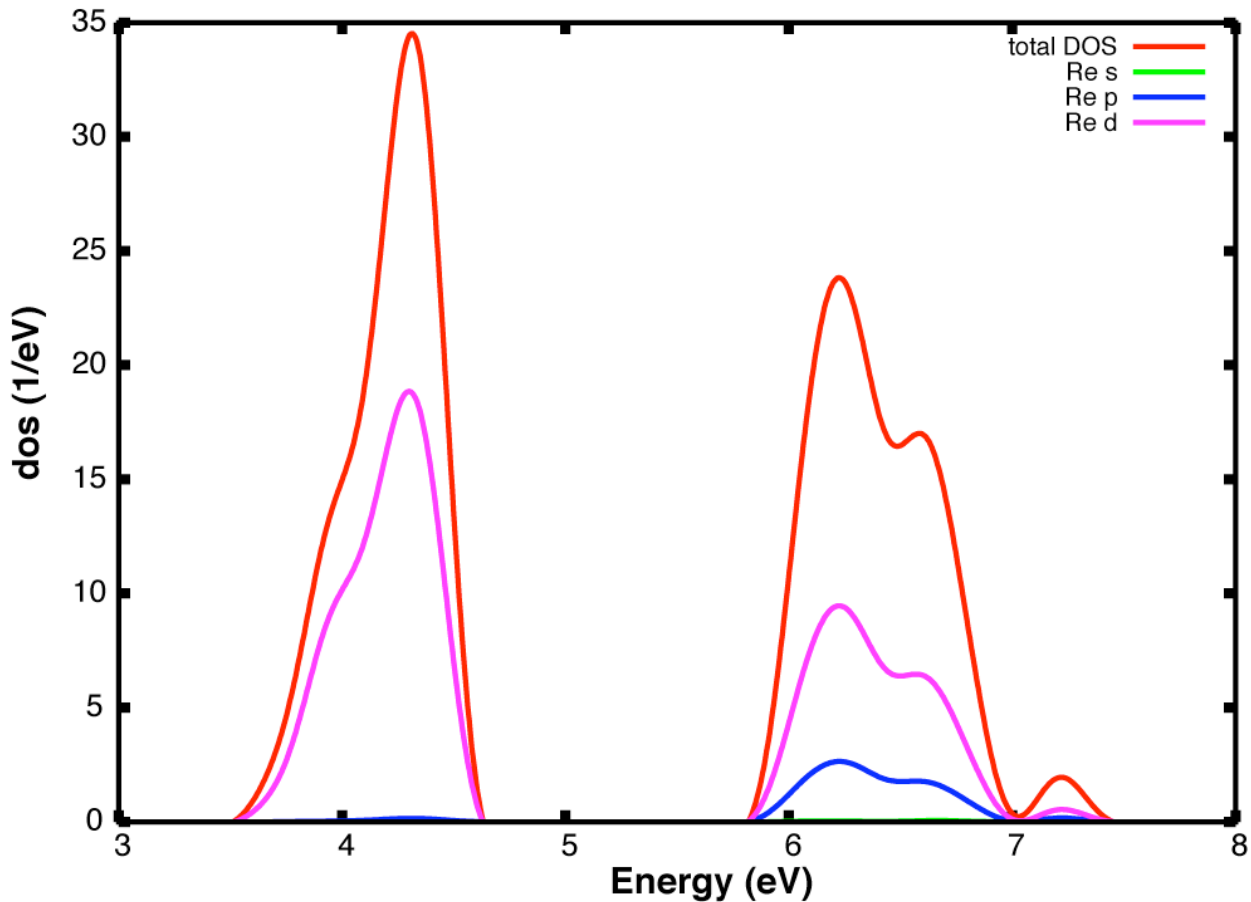


Figure S6. Density of unoccupied states for NaReO_4 crystal (red line) calculated using periodic boundary conditions with the VASP code and the hybrid density functional HSE in a plane wave expansion. The green, blue, and magenta lines indicate the percentage rhenium s, p, and d characters of the DOS resulting from projecting each band into a local basis set of spherical harmonic. The oxygen p component is not shown. While this picture is not indicative of the intensity in the xanes spectrum, it is indicative of the presence of three features resulting from hybridization of rhenium d and oxygen p orbitals. Notice that while the rhenium participation in the first peak in the DOS is almost entirely through d orbitals, a significant participation of p orbitals is observed in the second peak, similarly to what is shown in Figure S4 for the actual absorption spectrum.

Figure S7: Molecular orbitals for ReO_4^- calculated at the B3LYP optimized structure, $\text{Re}-\text{O}=1.751 \text{ \AA}$. (expt. $\text{Re}-\text{O}=1.722 \text{ \AA}$).

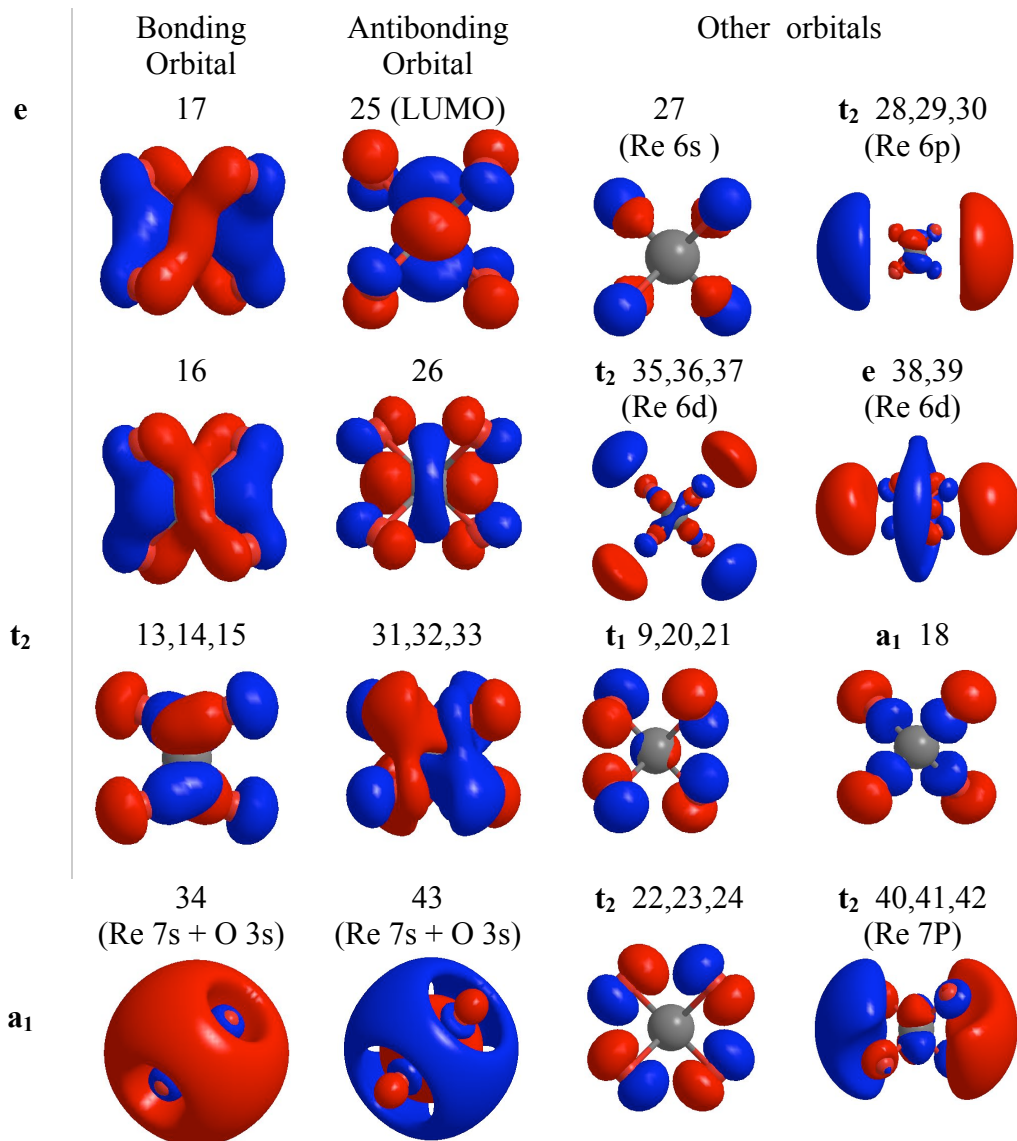


Table S1. The calculated bond lengths and charge for the optimized structure of the ReO_4^{1-} anion.

	M-O (Å)		Charge (Mulliken)	
	Expt. (ave.)	Calc.	Re	O
ReO_4^{1-}	1.722(5)	1.751	1.68	-0.67

Table S2. Orbital composition for representative occupied and unoccupied orbitals for ReO_4^- orbital contributions (B3LYP//Stuttgart, optimized structure, Gaussian 03).

MO #	Bond Sym	E. (eV)	Re_s	Re_p	Re_d	O s	O p
52,53,54	t ₂	31.65	0	0	0	0	100
49,50,51	t ₁	31.11	0	0	0	0	100
47,48	e	18.20	0	0	90	0	10
44,45,46	t ₂	16.22	0	0	90	0	10
43	a ₁	13.33	93.6	0	0	0	6.4
40,41,42	t ₂	9.99	0	100	0	0	0
38,39	e	6.50	0	0	94.1	0	6.0
35,36,37	t ₂	6.49	0	0	93.2	0	5.6
34	a ₁	6.04	98.4	0	0	0	1.6
31,32,33	t ₂	5.10	0	7.7	54.8	0	36.8
28,29,30	t ₂	3.92	0	95.4	3.8	0	0.4
27	a ₁	3.08	100	0	0	0	0
25, 26	e	3.03	0	0	60.9	0	38.8
LUMO							
22, 23, 24	t ₁	-3.21	0	0	0	0	100
HOMO							
19,20,21	t ₂	-4.05	0	6.0	4.0	0	89.2
18	a ₁	-5.40	0	9.4	0	0	84.8
16,17	e	-6.97	0	0	46.8	0	52.4
13, 14 15	t ₂	-7.03	0	4.3	34.5	0	54.8
10,11,12	t ₂	-20.16	0	1.4	5.8	91.6	0
9	a ₁	20.76	0	0	0	98.8	0
6,7,8	t ₂	-46.67	0	98.0	0	0	0.8
5	a ₁	-85.96	99.5	0	0	0	0
2,3,4	t ₂	-516.49	0	0	0	25.0	0
1	a ₁	-516.49	0	0	0	25.0	0

References

- (39) Bluhm, H. Andersson, K.; Araki, T.; Benzerara, K.; Brown, G. E.; Dynes, J. J.; Ghosal, S.; Gilles, M. K.; Hansen, H.-Ch.; Hemminger, J. C.; Hitchcock, A. P.; Ketteler, G.; Kilcoyne, A. L. D.; Kneedler, E.; Lawrence, J. R.; Leppard, G. G.; Majzlam, J.; Mun, B. S.; Myneni, S. C. B.; Nilsson, A.; Ogasawara, H.; Ogletree, D. F.; Pecher, K.; Salmeron, M.; Shuh, D. K.; Tonner, B.; Tyliszczak, T.; Warwick, T.; Yoon, T. H. *J. Electron Spectrosc. Relat. Phenom.* **2006**, *150*, 86.
- (40) Warwick, T.; Franck, K.; Kortright, J. B.; Meigs, G.; Moronne, M.; Myneni, S.; Rotenberg, E.; Seal, S.; Steele, W. F.; Ade, H.; Garcia, A.; Cerasari, S.; Denlinger, J.; Hayakawa, S.; Hitchcock, A. P. Tyiszcza, T.; Kikuma, J.; Rightor, E. G.; Shin, H.-J.; Tonner, B. P. *Review of Scientific Instruments*, **1998**, *69*, 2964.
- (52) Frisch, M. J. ; Trucks, G. W.; Schlegel, H. B.; Scuseria, G. E.; Robb, M. A.; Cheeseman, J. R.; J.A. Montgomery, J.; Vreven, T.; Kudin, K. N.; Burant, J. C.; Millam, J. M.; Iyengar, S. S.; Tomasi, J.; Barone, V.; Mennucci, B.; Cossi, M.; Scalmani, G.; Rega, N.; Petersson, G. A.; Nakatsuji, H.; Hada, M.; Ehara, M.; Toyota, K.; Fukuda, R.; Hasegawa, J.; Ishida, M.; Nakajima, T.; Honda, Y.; Kitao, O.; Nakai, H.; Klene, M.; Li, X.; Knox, J. E.; Hratchian, H. P.; Cross, J. B.; Bakken, V.; Adamo, C.; Jaramillo, J.; Gomperts, R.; Stratmann, R. E.; Yazyev, O.; Austin, A. J.; Cammi, R.; Pomelli, C.; Ochterski, J. W.; Ayala, P. Y.; Morokuma, K.; Voth, G. A.; Salvador, P.; Dannenberg, J. J.; Zakrzewski, V. G.; Dapprich, S.; Daniels, A. D.; Strain, M. C.; Farkas, O.; Malick, D. K.; Rabuck, A. D.; Raghavachari, K.; Foresman, J. B.; Ortiz, J. V.; Cui, Q.; Baboul, A. G.; Clifford, S.; Cioslowski, J.; Stefanov, B. B.; Liu, G.; Liashenko, A.; Piskorz, P.; Komaromi, I.; Martin, R. L.; Fox, D. J.; Keith, T.; Al-Laham, M. A.; Peng, C. Y.; Nanayakkara, A.; Challacombe, M.; Gill, P. M. W.; Johnson, B.; Chen, W.; Wong, M. W.; Gonzalez, C.; Pople, J. A., *Gaussian*, Rev. D.01; Gaussian Inc.: Wallingford, CT, 2004.